Available online at www.sciencedirect.com
ScienceDirect
Journal of the European Ceramic Society 29 (2009) 1477–1484
www.elsevier.com/locate/jeurceramsoc

Spark plasma sintering of lead phosphovanadate $Pb_3(VO_4)_{1.6}(PO_4)_{0.4}$

L. Campayo [a,*], S. Le Gallet [b], Yu. Grin [c], E. Courtois [a], F. Bernard [b], F. Bart [a]

[a] *CEA Marcoule, DTCD/SECM/LDMC, BP 17171, 30207 Bagnols sur Ceze Cedex, France*
[b] *Institut Carnot de Bourgogne, UMR 5209 CNRS-UB, 9 Av. Alain Savary, BP 47870, 210780 Dijon Cedex, France*
[c] *Max-Planck-Institut für Chemische Physik fester Stoffe Nötnitzer Strasse 40, 01187 Dresden, Germany*

Received 23 July 2008; received in revised form 11 September 2008; accepted 11 September 2008
Available online 26 October 2008

Abstract

Lead phosphovanadates can be used as reactants for the synthesis of iodoapatite. Because of its high chemical durability, iodoapatite has considerable potential interest for immobilizing radioactive iodine. Iodine-bearing compounds must be synthesized and consolidated at low temperatures to avoid iodine volatilization. Spark plasma sintering (SPS) thus appears to be a suitable sintering process because of its short processing time. This paper deals with spark plasma sintering of lead phosphovanadate powder prepared mechanically by attrition and planetary ball milling. The influence of sintering parameters such as the heating rate, temperature, and holding time on the degree of densification and the microstructure of bulk materials is discussed. The bulk characteristics were directly correlated with the shrinkage curves. The powder characteristics were determined (grain size and size distribution, specific area, crystallite size, etc.) to explain the singular sintering behavior of the attrited powder; we also investigated whether the latter exhibited the same singular behavior during conventional sintering and hot pressing.

Keywords: Lead phosphovanadate; Spark plasma sintering; Attrition; Iodine conditioning

1. Introduction

Lead phosphovanadates $Pb_3(VO_4)_{2(1-x)}(PO_4)_{2x}$ ($x = 0$ or 0.2) were used as reactants for synthesizing apatites $Pb_{10}(VO_4)_{6(1-x)}(PO_4)_{6x}I_2$[1] with good water leaching resistance.[2] These apatites are potentially of interest for immobilizing radioactive iodine arising from nuclear fuel reprocessing.[2,3] They are synthesized by calcining stoichiometric quantities of lead iodide and lead phosphovanadate according to the following equation:

$$3Pb_3(VO_4)_{2(1-x)}(PO_4)_{2x} + PbI_2 \rightarrow Pb_{10}(VO_4)_{6(1-x)}(PO_4)_{6x}I_2$$

Confined process conditions are necessary to prevent iodine volatilization above 500 °C. For this purpose, additional lead phosphovanadate was used to form an impermeable jacket around a $3Pb_3(VO_4)_{2(1-x)}(PO_4)_{2x} + PbI_2$ core.[4] This requires closure of the open porosity in the jacket prior to the beginning of iodine release, which occurs at about 450–500 °C (based on thermogravimetric analysis of the resulting iodine apatite[1–5]). This relative low temperature requires unconventional sintering techniques for densification of the jacket. Previous work on pressureless consolidation of attrition-milled $Pb_3(VO_4)_{2(1-x)}(PO_4)_{2x}$ powder ($S_{BET}(N_2) = 7.0\ m^2/g$)[6–8] showed that a temperature of at least 650 °C is necessary to exceed a relative density of 92%, the value above which open porosity is generally considered to have been eliminated. However, because of a phase transformation at 100 °C for $Pb_3(VO_4)_2$ ($P2_1/c \rightarrow R\bar{3}m$), the pellets with the composition $Pb_3(VO_4)_2$ remained brittle and this is why the present study was carried out with lead phosphovanadate $Pb_3(VO_4)_{1.6}(PO_4)_{0.4}$ for which the allotropic temperature is −50 °C.[9–11] In addition, to reduce the sintering temperature while allowing high heating rates, spark plasma sintering (SPS)[12–14] was found here to be an appropriate tool. This article aims at describing an experimental investigation of spark plasma sintering of lead phosphovanadate $Pb_3(VO_4)_{1.6}(PO_4)_{0.4}$.

2. Experimental procedures

2.1. Powder synthesis and characterization

$Pb_3(VO_4)_{1.6}(PO_4)_{0.4}$ powder was obtained by mixing and calcining the stoichiometric powder mixture of PbO (99.3% purity, Prolabo, France), V_2O_5 (99.2% purity, Alfa Aesar,

* Corresponding author.
E-mail address: lionel.campayo@cea.fr (L. Campayo).

0955-2219/$ – see front matter © 2008 Elsevier Ltd. All rights reserved.
doi:10.1016/j.jeurceramsoc.2008.09.003

Germany) and $NH_4H_2PO_4$ (97.5% purity, Prolabo, France) at 1000 °C for 1 h. The obtained powder, was ground in water for 210 min in a planetary ball mill (PM400, Retsch) in a tungsten carbide bowl or for 240 min in an attrition mill (Attritor 01-HD, Union Process) in a zirconia bowl. These powders were then dried at 100 °C. The resulting powders were designated P1 (planetary ball milling) and P2 (attrition milling); their specific surface areas as determined by the BET method (GEMINI 2360, Micromeritics) were 1.0 and 8.0 m^2/g, respectively. The samples were characterized by X-ray diffraction (Siemens D5000), which showed that P2 powder contained not only lead phosphovanadate but also traces of lead hydroxyvanadinite, $Pb_{10}(VO_4)_{4.8}(PO_4)_{1.2}(OH)_2$. This latter compound was likely formed during the drying for which higher water amounts were to evaporate for P2 powder (pseudo-hydrothermal synthesis conditions). Thermogravimetric analyses (heating rate of 10 °C/min) on $Pb_3(VO_4)_{1.6}(PO_4)_{0.4}$ and $Pb_{10}(VO_4)_{4.8}(PO_4)_{1.2}(OH)_2$ taken separately showed that lead phosphovanadate was stable up to its melting at 960 °C whereas lead hydroxyvanadinite presented two states of weight loss respectively between 100–370 and 370–500 °C. The crystallite sizes of 40 and 20 nm for powders P1 and P2 respectively were estimated from the powder diffraction patterns applying the Langford method.[15] Laser particle size analysis (Coulter LS 130 and Malvern Zetasizer Nano-ZS) was also carried out in distilled water with a dispersing agent (Dolapix ET 85, Zschimmer et Schwarz). Powder P1 had a broad particle size distribution comprising four grain populations centered around 10, 3.5, 0.7 and 0.14 μm, whereas powder P2 was characterized by a narrower distribution with a main population centered around 0.3 μm and fine one centered around 0.15 μm. These results were confirmed by SEM observations of the powders using a JEOL JSM-6400F apparatus (Fig. 1). Powder P2 was also annealed in air for 15 min at 400 °C in a quartz vessel. The annealed P2 powder (designated P2A) still contained traces of lead hydroxyvanadinite, but exhibited characteristics slightly different from the original P2 powder. After heat treatment, its specific surface area decreased from 8.0 to 5.2 m^2/g together with the grain size (fines from 0.15 to 0.11 μm for example), while the crystallites increased in size from 20 to 40 nm.

The structural and morphological characterizations suggest that (i) the P1 powder grains consisted of relatively dense aggregates (0.14–10 μm) of 40 nm crystallites; (ii) the P2 powder grains were porous aggregates (0.15–0.3 μm) of 20 nm crystallites; and (iii) annealing the P2 powder resulted in densification of the aggregates and growth of the crystallites.

2.2. Sintering conditions and characterization of sintered materials

Powders P1 and P2 (6.48 g) were sintered in graphite molds (15 mm inside diameter) by spark plasma sintering (SPS 515S, Syntex Inc.). The effects of temperature, residence time and heating rate were evaluated, but not the effect of pressure. Because of the brittleness of lead phosphovanadate, the pressure was maintained at 30 MPa during the experiments. All the tests are summarized in Table 1. Powder P2 was in addition sintered by uniaxial hot pressing (HP) under the same conditions as sample P2-5 (670 °C, 50 °C/min, 5 min, 30 MPa). A sample of the same powder after uniaxial cold-pressing at 100 MPa was sintered (10 °C/min) in a dilatometry apparatus (Setaram SetSys TMA 16/18). Annealed P2 powder (P2A) was sintered by SPS under the same conditions as sample P2-3 (600 °C, 50 °C/min, 5 min, 30 MPa). In addition, a composite comprising a cylindrical core of iodoapatite $Pb_{10}(VO_4)_{4.8}(PO_4)_{1.2}I_2$ pelletized by uniaxial cold compaction at 80 MPa, surrounded by a lead phosphovanadate jacket (P2 powder), was sintered by SPS (Sumitomo SPS 2080, PNF^2, Toulouse, France) under the same conditions as sample P2-4 (630 °C, 50 °C/min, 5 min, 30 MPa).

The density of all the samples was measured by hydrostatic weighing. The samples were chemically etched by 0.05 M nitric acid to reveal the grain boundaries for observation by scanning electron microscopy (Philips, XL30 W-TMP). According to the X-ray powder diffraction data, $Pb_3(VO_4)_{1.6}(PO_4)_{0.4}$ phase was conserved during sintering. The theoretical density of this compound determined by X-ray diffraction was[7] 7.302 g cm^{-3} and the relative density of the obtained ceramics gives the ratio between the hydrostatic density and the X-ray density.

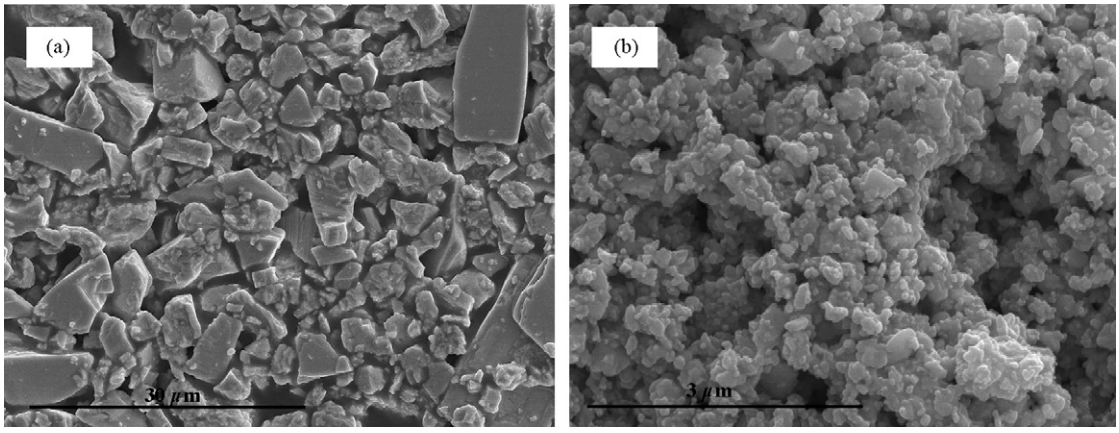

Fig. 1. SEM images of the powders (a) P1 and (b) P2.

Table 1
Lead phosphovanadate sintering experiments. The external pressure was 30 MPa for each test. The designation P1 or P2 refers to the milling method used. The designation P2A indicates annealed P2 powder. SPS: spark plasma sintering; HP: hot pressing.

Experiment	Dwell temperature (°C)	Dwell time (min)	Heating rate (°C/min)	Relative density (%)
Effect of dwell temperature				
P1-1 (SPS)	400	5	50	64.7 ± 0.2
P2-1 (SPS)	400	5	50	61.9 ± 0.2
P1-2 (SPS)	500	5	50	72.2 ± 0.1
P2-2 (SPS)	500	5	50	91.1 ± 0.2
P1-3 (SPS)	600	5	50	90.8 ± 0.5
P2-3 (SPS)	600	5	50	98.2 ± 0.4
P2A-3 (SPS)	600	5	50	98.0 ± 0.4
P1-4 (SPS)	630	5	50	95.2 ± 0.2
P2-4 (SPS)	630	5	50	97.9 ± 0.1
P1-5 (SPS)	670	5	50	97.8 ± 0.3
P2-5 (SPS)	670	5	50	97.0 ± 0.3
Effect of dwell time				
P2-6 (SPS)	400	20	50	61.7 ± 0.4
P2-7 (SPS)	500	20	50	97.6 ± 0.3
Effect of heating rate				
P2-8 (SPS)	630	5	200	93 ± 0.2
P2-9 (SPS)	670	5	200	92.5 ± 0.6
Comparative hot pressing test				
P2-5 (HP)	670	5	50	95.6 ± 0.1

3. Results and discussion

Fig. 2 shows the shrinkage of powders P1 and P2 versus the sintering temperature. Experiment P1-1 (sintering at 400 °C) is not shown because no significant shrinkage was observed. Stronger shrinkage was observed in all experiments for P2 powder comparing to the P1 powder. As shown by the sample densities (Table 1), this result does not mean that the P1 powder sintering conditions resulted in lower sample densities (relative densities above 90% were obtained for both powders). This result simply demonstrates that same mass of P1 and P2 powders pelletized at the same pressure (30 MPa) result in different green relative densities (consistent with published data by Robin et al.[8] on these powders), and thus to different pellet heights before sintering. Powder P2, with a finer particle size and narrower size distribution, being, in addition, formed by porous aggregates, was more difficult to compact than P1 powder and exhibited greater shrinkage for a comparable relative density after sintering. Sintering of P2 powder samples began at 240 °C, whereas with P1 powder, sintering began only at about 420 °C. This might be caused by thermal decomposition of the lead hydroxyvanadinite at low temperatures. Indeed, on the basis of the comparison with the apatitic phases $Ca_{10}(PO_4)_6(OH)_2$ and $Pb_{10}(PO_4)_6(OH)_2$,[16] the decomposition of lead hydroxyvanadinite can be written as follows:

$$Pb_{10}(VO_4)_{4.8}(PO_4)_{1.2}(OH)_2 \rightarrow Pb_{10}(VO_4)_{4.8}(PO_4)_{1.2}(OH)_{2-x}O_{x/2} + (x/2)H_2O$$

$$Pb_{10}(VO_4)_{4.8}(PO_4)_{1.2}(OH)_{2-x}O_{x/2} \rightarrow (3-y)Pb_3(VO_4)_{1.6}(PO_4)_{0.4} + (1-y)Pb_4(VO_4)_{1.6}(PO_4)_{0.4}O + (1-y)PbO + ((2-x)/2)H_2O$$

This two-step mechanism is consistent with the two states of weight loss determined by thermogravimetric analysis (see Section 2.1) and with the two gas releases observed during the SPS sintering of P2 powder samples (see Fig. 3, chamber pressure). However, the sintering of P2 powder samples (P2-4, P2-5, P2-8, and P2-9) began always at 240 °C although the lead hydroxyvanadinite decomposition temperature depended on the heating rate and was shifted to higher temperatures when the heating rate increased (see Fig. 3). In this way, for these conditions, powder granulometry effect is thus the only possible phenomenon to explain different initial sintering temperatures between powder P1 and P2. Table 1 shows that the same relative density of 91% was reached at 500 °C for P2 compared with 600 °C for P1. As expected, the powder granulometry has a fundamental role in

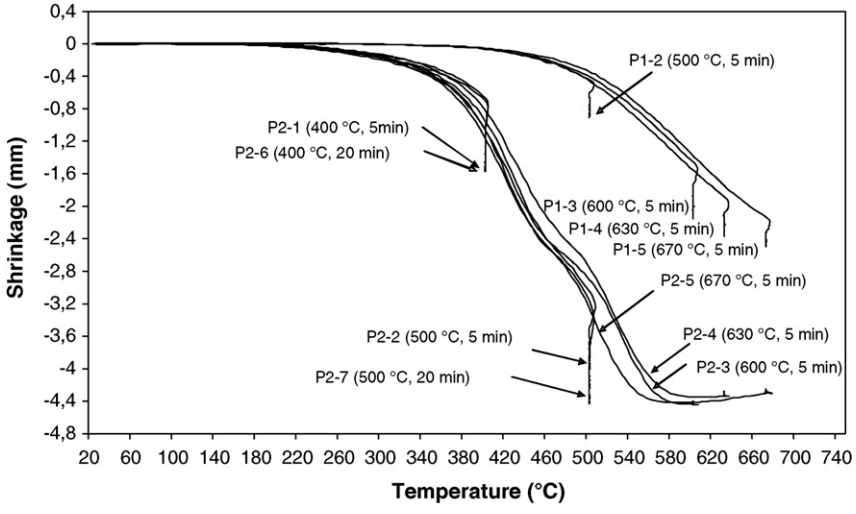

Fig. 2. Effect of temperature and dwell time on shrinkage of powders P1 and P2 for temperatures: 400 and 500 °C.

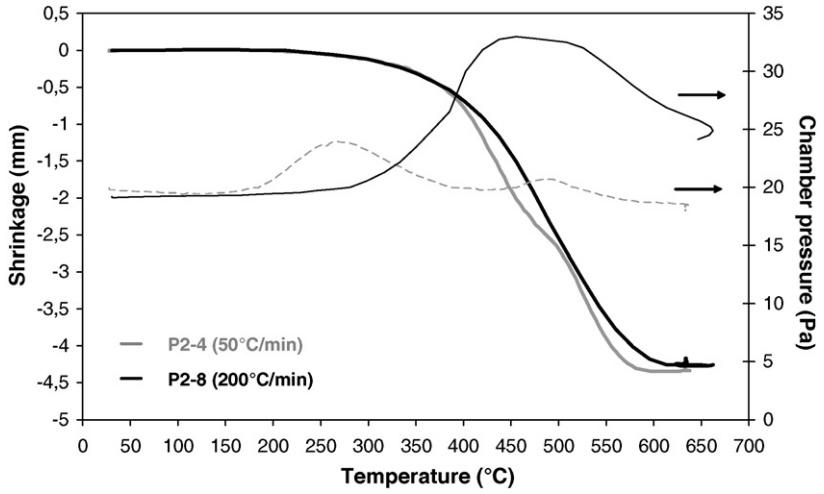

Fig. 3. Effect of heating rate on shrinkage of P2 powder and chamber pressure at a dwell temperature of 630 °C.

the densification mechanisms and the small particle size tends to shift the sintering toward lower temperatures. Analysis of the diffraction patterns by the Langford method showed that the crystallite size in the P2 powder samples increased from 20 to 30 nm when they were sintered at 670 °C. In contrary, no change was observed in the size of the crystallites in sintered P1 samples.

Fig. 2 (P2-1 (SPS), P2-6 (SPS), P2-2 (SPS), P2-7 (SPS)) also illustrates the effect of the dwell time on the shrinkage of P2 powder at temperatures: 400 and 500 °C. The dwell time affected densification only at 500 °C. Moreover, sintering for 20 min at 500 °C was equivalent in terms of shrinkage to the sintering for 5 min at 600 °C (see also Table 1). SEM observation of the samples showed that increasing the dwell time for sintering temperatures of 400 and 500 °C did not affect the grain size: the initial size was conserved whatever the dwell time.

Fig. 3 illustrates the effect of the heating rate on shrinkage of P2 powder sintered at 630 °C (the same trend is observed for a sintering temperature of 670 °C). While the temperature at which sintering begins does not appear to be affected by the heating rate, the total temperature interval for a same shrinkage increases with the heating rate. Lower density was obtained when the heating rate was increased from 50 to 200 °C/min. This trend could be attributed to (i) shorter exposure to the sintering temperature range as the heating rate increases and (ii) slight gas release observed during sintering. The first gas release occurred between 200 and 300 °C at a heating rate of 50 °C/min (Fig. 3) but was shifted toward higher temperatures when the heating rate was increased to 200 °C/min. The temperature range in which it occurs corresponds to closure of the open porosity, trapping in this way a fraction of the gas. Finally, gas trapping and a shorter sintering time probably does not allow densification as high as 98.2% (the relative density of P2-3 (SPS)) with such high heating rates.

The shrinkage and density variations versus temperature indicate a slight decrease in density at sintering temperatures above 600 °C in the case of P2 powder. This phenomenon was not observed for P1 powder. The amplitude of the dedensification of P2 powder observed on the shrinkage curves when the sintering temperature exceeded 600 °C is consistent with the density variations in Table 1.

SEM observations of polished and etched cross sections revealed that the initial grain size of P2 powder (0.3 μm) was conserved in the compacts as long as the sintering temperature was lower than 600 °C. A second population with a grain size

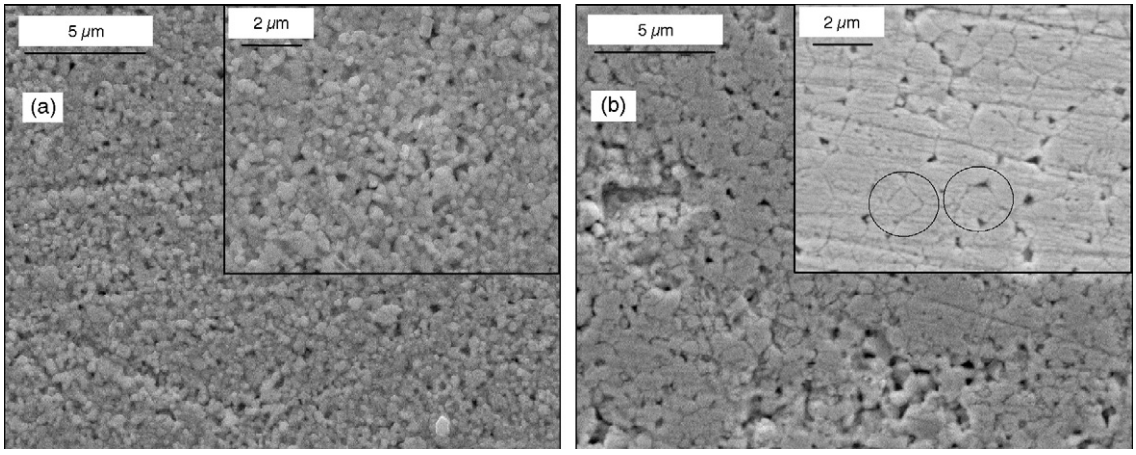

Fig. 4. SEM images showing the effect of the heating rate on growth of P2 powder grains: (a) heating rate of 50 °C/min and (b) heating rate of 200 °C/min.

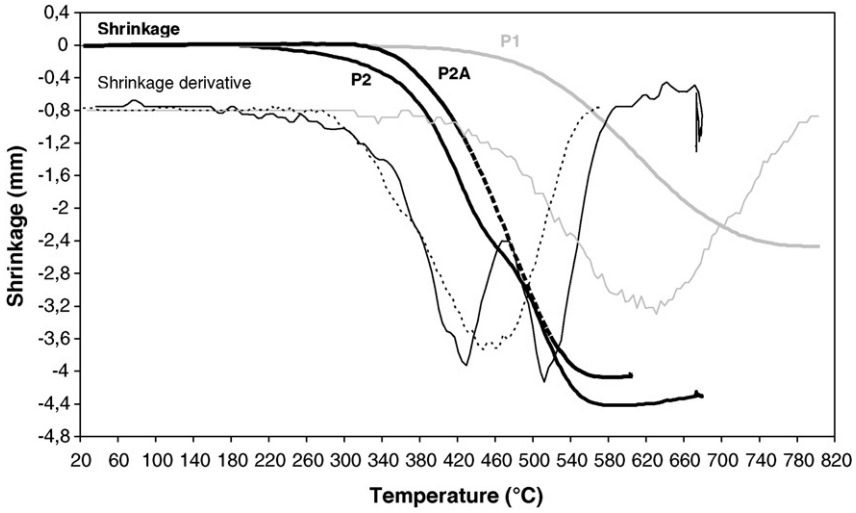

Fig. 5. Singular behavior of P2 powder (for example P2-5 (670 °C, 5 min)) compared with P1 and P2A powder.

centered on 1 μm appeared at higher temperatures (like in the right photo in Fig. 4). The proportion of the new grain population increased when the sintering temperature was raised from 630 to 670 °C. For the smaller grains (0.15 μm) the microscope resolution and their small fraction in the material made it impossible to determine their evolution during sintering. No significant difference in the grain size of the compacts was observed versus temperature with P1 powder, although the broad initial particle size distribution made it difficult to identify size variations. The greater the dedensification, the larger the population of 1 μm grains in the samples. This is probably caused by Ostwald ripening due to the consumption of lead phosphovanadate crystal nuclei fathered by the decomposition of lead hydroxyvanadinite. Dedensification was also observed in samples when the heating rate was increased to 200 °C/min. The particle growth identified by SEM observation of polished cross sections after chemical etching was then of greater amplitude (Fig. 4): the population of 1 μm grains increased with respect to a sample sintered with a heating rate of 50 °C/min, all other conditions being equal; it also began at a lower sample density than observed with a slower heating rate. This factor also limited the final consolidation of the specimens sintered at 200 °C/min. However the overheating on reaching the dwell temperature was 27 °C at a heating rate of 200 °C/min, compared with only 6 °C for a rate of 50 °C/min. Assuming the temperature-dependence of the particle growth, the lower density can most likely be attributed to this overheating rather than to the actual increase in the heating rate.

Fig. 5 reveals the unusual SPS behavior of P2 powder compared with P1 and P2A. P2 powder sintering is characterized by two maximum shrinkage rates corresponding to two minima of the first derivative of shrinkage with respect to temperature (or time, given the linear relation between these two parameters) at 420 and 510 °C. Increasing the heating rate shifts the shrinkage minima toward higher temperatures (420 °C → 465 °C; 510 °C → 525 °C) but decreases the temperature difference between them. Irrespective of the heating rate,

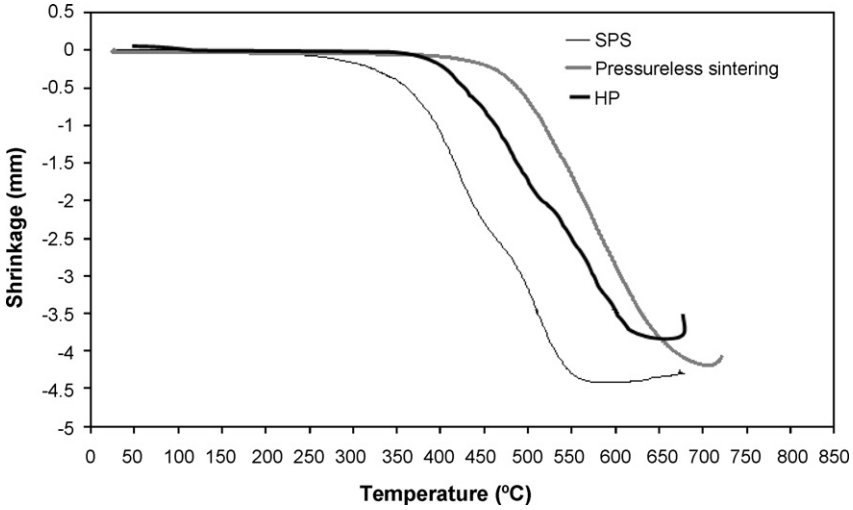

Fig. 6. Shrinkage of the SPS treated sample (P2-5 (670 °C, 5 min)) in comparison with HP and pressureless consolidation.

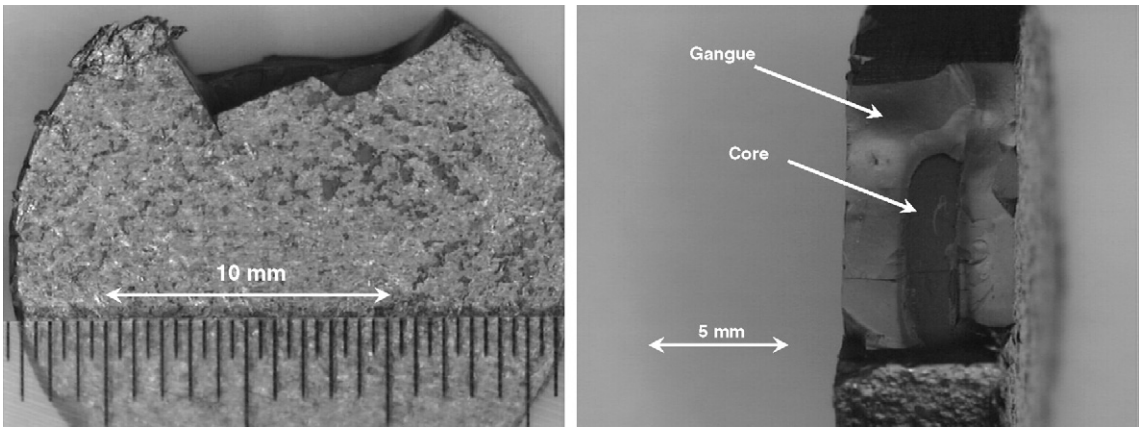

Fig. 7. $Pb_{10}(VO_4)_{4.8}(PO_4)_{1.2}I_2/Pb_3(VO_4)_{1.6}(PO_4)_{0.4}$ composite sintered for 5 min at 630 °C (50 °C/min) at 30 MPa.

two-step shrinkage does not appear to be specific to spark plasma sintering conditions; Fig. 6 compares the P2 powder shrinkage observed for conventional sintering, SPS, and uniaxial hot pressing (HP), and shows that in the latter case the same singular behavior is observed as for SPS. Such behavior is not observed for conventional sintering of P2 powder or for spark plasma sintering of P1 and P2A powders, for which a single maximum shrinkage rate is observed at 620 and 460 °C, respectively.

Two-step shrinkage as in the case of spark plasma sintered P2 powder has already been observed for other materials such as yttriated zirconia. One explanation advanced by some authors[17] relates the two steps to the closure of a type of porosity: open porosity followed by closed porosity. In our test, however, a fraction of the open porosity still appears to be eliminated during the second step (see *Composite sintering* below). We therefore propose another interpretation for this phenomenon in relation with the structural and morphological characteristics of the test powders. As P2 powder is characterized by porous aggregates, shrinkage variations can reflect internal densification and rearrangement of the aggregates (first macroscopic shrinkage) followed by a second step of inter-aggregate densification. For powders P2A and P1, characterized by aggregates of dense crystallites, only the inter-aggregate densification step occurs. Rearrangement of the aggregates is probably activated by the external pressure applied to the system. This explains why no rearrangement occurs after intra-aggregate densification in the case of conventional pressureless sintering, and why only a single macroscopic shrinkage step corresponding to inter-aggregate densification is observed.

An illustration of the composite sintered at 630 °C for 5 min is shown in Fig. 7. Fig. 8 plots the shrinkage of the jacket material alone or with an iodoapatite core versus the temperature. Sintering of the composite involves the two-step densification mechanism and dedensification above 600 °C, both of which are also observed for sintering of the jacket alone. The dedensification is slightly more evident however. Fig. 9 shows the pressure variations in the furnace chamber versus the temperature for the jacket material alone and for the composite. We calculated the ratio of the areas under the curve between 140 and 420 °C and between 420 and 580 °C corresponding to the two gas release regions; the values were 8.4 for the jacket alone and 0.97 in the composite, suggesting that the core is responsible for the

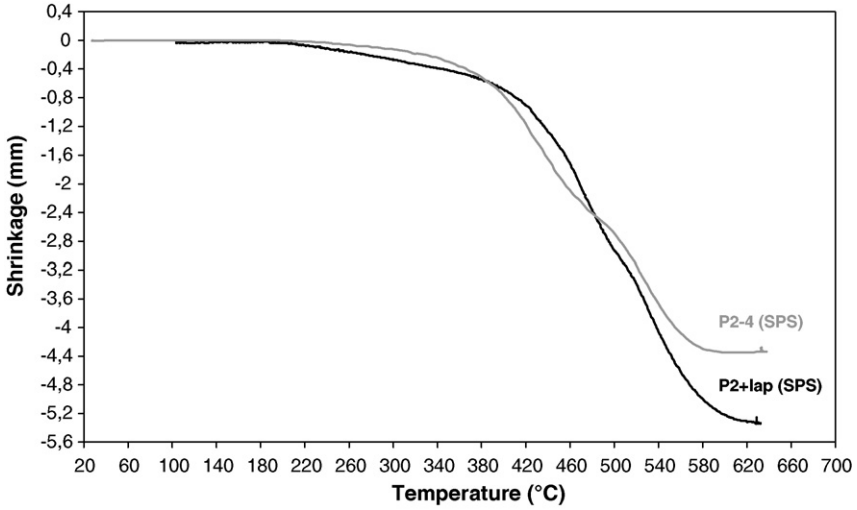

Fig. 8. Shrinkage variations during sintering of jacket material alone (P2-4 (630 °C, 5 min)) or with an iodoapatite core (P2 + iodoapatite).

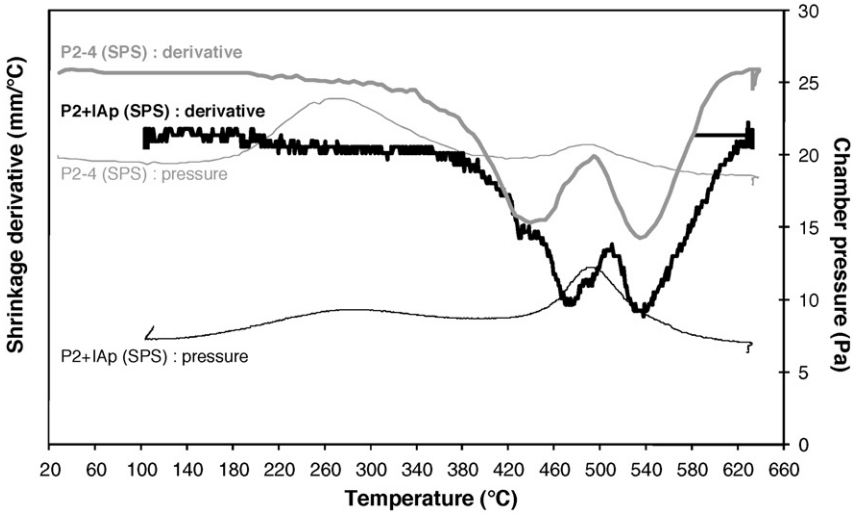

Fig. 9. Shrinkage derivatives and pressure variations in the furnace versus temperature for jacket material alone (P2-4 (630 °C, 5 min)) and for composite (P2 + iodoapatite).

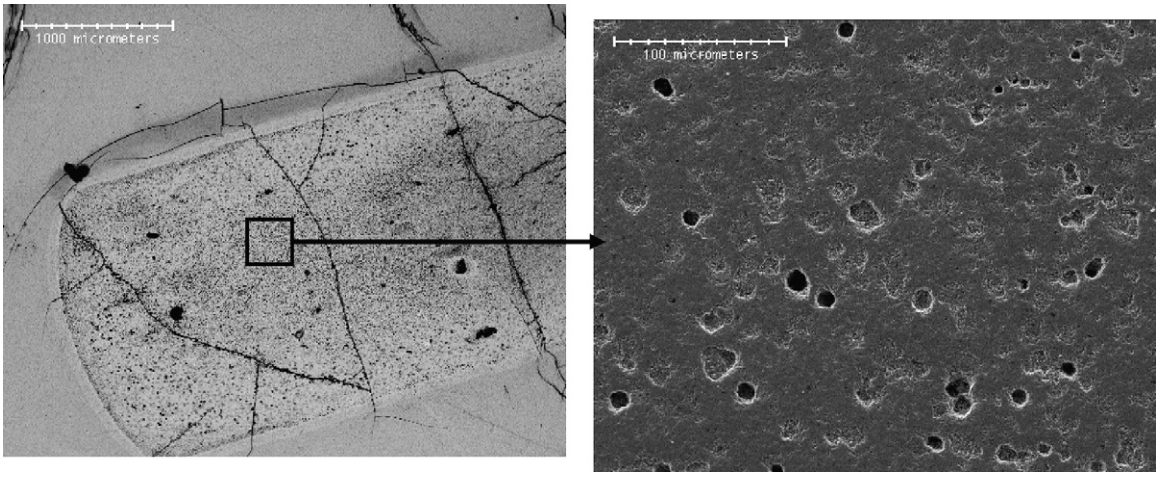

Fig. 10. SEM images of $Pb_{10}(VO_4)_{4.8}(PO_4)_{1.2}I_2/Pb_3(VO_4)_{1.6}(PO_4)_{0.4}$ composite sintered for 5 min at 630 °C (50 °C/min) at 30 MPa.

pressure rise between 420 and 580 °C. Iodoapatite is known to decompose with iodine loss at atmospheric pressure within this temperature range,[1] which is consistent with our observations. Fig. 9 shows the shrinkage derivative versus the temperature for the jacket material alone and for the composite. The composite curve includes four accidents at 440, 470, 490 and 530 °C. The peaks at 440 and 530 °C correspond to the two steps identified for sintering of the jacket material alone. The pressure rise inside the furnace due to iodoapatite decomposition is observed beyond the first minimum of the first derivative of jacket material shrinkage, suggesting that the open porosity was not fully eliminated during the first shrinkage step.

SEM observations (Fig. 10) show that the jacket is characterized by a dense microstructure consistent with the previous results, and that the core is porous (macropores measuring about 10 μm) and cracked. The microstructure of the core is responsible for the mechanical brittleness of the composite and also confirms the iodoapatite decomposition. This results in iodine overpressure in the sample once the open porosity of the jacket has been closed (second shrinkage step).

4. Conclusion

A parameter study of spark plasma sintering of lead phosphovanadate, $Pb_3(VO_4)_{1.6}(PO_4)_{0.4}$, identified a strong correlation between the structural characteristics of the powders and the shrinkage behavior. If the powder consists of porous aggregates about 0.3 μm in diameter, i.e. after attrition milling, shrinkage becomes a two-step process: the first step consists in eliminating the intra-aggregate porosity followed by rearrangement of the aggregates due to the external pressure applied; the second involves the elimination of inter-aggregate porosity. A maximum relative density of 98.2% was obtained after sintering for 5 min at 600 °C with a heating rate of 50 °C/min. Dedensification of the sintered materials was observed at temperatures exceeding 600 °C, initiated by the appearance of a grain population with a particle size of about 1 μm. To avoid this particle growth phenomenon while conserving high relative densities, the dwell time can be increased within the temperature range corresponding to the second shrinkage step by sintering for 20 min at 500 °C. This appears to be compatible with the

thermal stability of iodoapatite, for which lead phosphovanadate can be used as a diffusion barrier during sintering. On the contrary, with its particle size distribution and the resulting sintering temperature range, P1 powder cannot be used as a jacket material for iodine immobilization. At higher temperatures the decomposition of the apatite phase generates iodine overpressure in the core of iodoapatite/lead phosphovanadate composites. The jacket sintering behavior differs from that of the core. The maximum iodoapatite shrinkage rate appears between the two jacket shrinkage steps at temperatures ranging from about 470–490 °C. It should therefore theoretically be possible to perform spark plasma sintering of iodoapatite without a diffusion barrier at temperatures below the decomposition value.

References

1. Audubert, F., Mise au point d'une matrice apatitique pour le confinement de l'iode 129, PhD Thesis, Institut National Polytechnique de Toulouse, Toulouse, France, 1995.
2. Guy, C., Audubert, F., Lartigue, J. E., Latrille, C., Advocat, T. and Fillet, C., New conditionings for separated long-lived radionuclides. *Comptes Rendus Physique*, 2002, **3**(7–8), 827–837.
3. Maddrell, E. R. and Abraitis, P. K., A comparison of wasteforms and processes for the immobilization of iodine-129. Proceedings of Scientific Basis for Nuclear Waste Management—XXVII. *Materials Research Society Symposium Proceedings*, 2004, **807**, 261–266.
4. Audubert, F., Carpena, J., Lacout, J. L. and Tetard, F., Elaboration of an iodine-bearing apatite—iodine diffusion into a $Pb_3(VO_4)_2$ matrix. *Solid State Ionics*, 1997, **95**(1–2), 113–119.
5. Uno, M., Shinohara, M., Kurosaki, K. and Yamanaka, S., Some properties of a lead vanado-iodoapatite $Pb_{10}(VO_4)_6I_2$. *Journal of Nuclear Materials*, 2001, **294**(1–2), 119–122.
6. Robin, T., Bernache-Assollant, D. and Audubert, F., Influence of vanadium substitution on sintering behaviour of $Pb_3(VO_4)_{2(1-x)}(PO_4)_{2x}$ ceramics. *Journal of the European Ceramic Society*, 2000, **20**(9), 1231–1240.
7. Robin, T., Étude du frittage de la solution solide $Pb_3(VO_4)_{2(1-x)}(PO_4)_{2x}$ dans le cadre du conditionnement de l'iode 129, PhD Thesis, Université de Limoges, Limoges, France, 2000.
8. Robin, T., Bernache-Assollant, D. and Audubert, F., Influence of grinding method on $Pb_3(VO_4)_{1.6}(PO_4)_{0.4}$ sinterability. *Powder Technology*, 1999, **103**(1), 10–18.
9. Kiat, J. M., Garnier, P., Calvarin, G. and Pinot, M., Structural study of lead orthophosphovanadates: role of the electron lone pairs in the phase transitions. *Journal of Solid State Chemistry*, 1993, **103**, 490–503.
10. Kiat, J.M., Étude par diffraction des rayons X des états métastables générés au cours des transitions de phases du Niobate de baryum et de sodium et des phosphovanadates de plomb: influence des défauts et des coexistences de phases, PhD Thesis, Université Paris VI, Paris, France, 1988.
11. Kiat, J. M., Calvarin, G., Garnier, P. and Gregoire, P., Ferroelastic phase transitions in lead orthophosphovanadates $Pb_3P_{2x}V_{2-2x}O_8$. *Japanese Journal of Applied Physics*, 1985, **24**, 690–692.
12. Tokita, M., Trends in advanced SPS spark plasma sintering systems and technology. *Journal of the Society of Powder Technology, Japan*, 1993, **30**, 790–804.
13. Omori, M., Sintering, consolidation, reaction and crystal growth by the spark plasma system (SPS). *Materials Science and Engineering A*, 2000, **287**(2), 183–188.
14. Millot, N., Le Gallet, S., Aymes, D., Bernard, F. and Grin, Yu., Spark plasma sintering of cobalt ferrite nanopowders prepared by coprecipitation and hydrothermal synthesis. *Journal of the European Ceramic Society*, 2007, **27**(2–3), 921–926.
15. Langford, J. L., *Accuracy in Powder Diffraction II*, *846*, ed. E. Prince and J. K. Stalick. NIST spec. Pub., Gaitherburg, M.D., May 26–29, 1992, p. 40.
16. Elliott, J. C., *Studies in Inorganic Chemistry 18: Structure and Chemistry of the Apatites and other Calcium Orthophosphates*. Elsevier, Amsterdam (The Netherlands), 1994, pp. 127–133.
17. Guizard, C., Bernard-Granger, G. and Monchalon, N., Étude du frittage SPS d'une poudre de zircone ultrafine. In *Proceedings of Matériaux 2006*, 2006 [Conference CM-08-0721].